The Circadian Clock Ensures Successful DNA Replication in Cyanobacteria

Yi Liao and Michael J. Rust

Supplementary information

Contents

I. Strain construction

Molecular cloning with *Synechococcus elongatus* PCC 7942 was carried out using standard protocols (1). Strains and plasmids are listed in Tables S1 and S2. Primers used for strain construction are listed in Table S3.

The TetO/TetR strain used for chromosome counting (Fig. S2) requires careful handling, as the operator array was prone to be lost due to genetic instability. We do not make frozen stocks for this strain since several days of growth in liquid culture can result in complete loss of detectable foci. Instead, it is better to make frozen stocks for the TetR-only strain (MRC1219) first. Approximately a week prior to imaging, these cells were transformed with the TetO plasmid (pMR0212) to make the complete TetO/TetR system (MRC1220). ~5 μg/ml of anhydrotetracycline was also added during transformation to mitigate growth defects. After antibiotic selection on BG11 plates, individual colonies were further selected and propagated in BG11 liquid culture (with the appropriate antibiotics) for a maximum of 2 days before being harvested for imaging.

To visualize the position and dynamics of replication proteins with time-lapse microscopy, we fused the fluorescent protein gene *egfp* at native genetic loci of various proteins involved in DNA replication. Each strain was made by transforming wildtype (WT) or clock-mutant *S. elongatus* cells with a plasmid carrying the desired construct. Each plasmid contained 5 fragments assembled together using Gibson assembly (2): an EcoRI-digested pBlueScript II SK (+) plasmid backbone, a 1 kb sequence upstream of the gene of interest (GOI) along with the GOI itself, the *egfp* sequence, a spectinomycin resistance (Sp^R) cassette, and a 1 kb sequence downstream of GOI. All insertions were verified by PCR and Sanger sequencing. Through homologous recombination between the bacterial genome and the 1 kb flanking sequences, the GOI-*egfp*-Sp^R construct was incorporated into the bacterial genome at the native locus of the GOI and verified by PCR.

We tested the signal qualities of 7 EGFP-fused proteins, which were DnaA, DnaB, SSB, β subunit (encoded by the *dnaN* gene), δ subunit, δ' subunit and τ subunit. Among these, only SSB and the β subunit, which have the highest stoichiometries at the replication fork (3), produced signal-to-noise ratios good enough for visualization and analysis. This is likely due to

the exceptionally high background fluorescence from various types of pigments present in the cyanobacteria cytosol.

The GalP-expression plasmid (pMR0210) was made by Gibson-assembling the sequence of a constitutive *p*GlnB promoter and the sequence of *galp* between the SalI and XbaI restriction sites of plasmid pAM1579 that targets the neutral-site II (NS2.1) of the *S. elongatus* genome. pMR0210 was then transformed into appropriate strains for visualization of β-EGFP and EdU with glucose feeding.

II. Cell culture for EdU Alexa Fluor 488 imaging and replisome time-lapse imaging

S. elongatus does not have a naturally intact nucleotide salvage pathway and is expected to be unable to incorporate thymidine analogs (e.g., EdU and BrdU) into the chromosome. To enable EdU labeling of replication sites, we used an engineered strain that expresses herpes simplex virus type-1 thymidine kinase (TK) from an IPTG-inducible promoter (plasmid was a gift from the Yoshikawa Lab) (4). As basal expression of TK from the leaky promoter was sufficient for visualization, no IPTG was added in our experiments.

S. elongatus cultures were grown in BG11M liquid medium at 30 °C with shaking, under an ambient light intensity of ~30 μmol photons m^{-2} s^{-1} provided by cool white fluorescent light bulbs (Philips Alto II). Cells were harvested at OD_{750} ~0.1–0.4, diluted back to OD_{750} = 0.1, pipetted into a 96-well plate and placed in a 30 °C incubator with shaking. Above each well of the 96-well plate is a red LED driven by a microcontroller that allows a user-defined temporal pattern of illumination (5). To image EdU as a function of circadian time, we entrained cells to 12 phases spanning 24 hours (θ = 0, 2, … 22 hours) by dividing LEDs into 12 groups, where each group generated 2 consecutive light/dark (LD) cycles (for a total of 48 hours) that phase-lags the preceding group by 2 hours. By the time all groups have completed the LD entrainment and have been grown in constant light (LL) for at least another 24 hours, cells from each group were incubated with 50 μM EdU in LL for 10 minutes before being fixed with 3.7% formaldehyde in 1x phosphate-buffered saline (PBS) for 15 minutes at room temperature (RT). After a wash step with 1% bovine serum albumin (BSA) in PBS, cells were permeabilized at RT with 0.05% Triton X-100 in PBS for 15 minutes and then 0.2 mg/mL lysozyme in 1x TE buffer for 30 minutes. Next, cells were washed again with 1% BSA in PBS, and click chemistry

between EdU and Alexa Fluor 488 (6) was performed according to the manufacturer instructions provided with the EdU imaging kit (Invitrogen). To remove unbound dye molecules, another washing step with 1% BSA was performed after the reaction. Cells from different groups were resuspended in 1x PBS, and 1 μL from each condition was used for imaging.

EdU imaging in the dark were performed similarly, except that cells were harvested at 2-hour intervals starting at lights-out ($t = 0$), and pulse-labeling was performed in the dark.

To correct for false positives in EdU Alexa Fluoro 488 imaging, a separate batch of cells was prepared where cells were subject to the same sample preparation and imaging procedures except that no EdU treatment was given. We estimated that the average false positive rate was 0.0036 counts/μm, which was subtracted from all reported values in this study.

The temperature, light intensity and growth medium for culturing the β-EGFP and SSB-EGFP strains for replisome time-lapse microscopy were identical to those used for the thymidine kinase strain.

III. Microscopy and image processing

Cells from each condition was resuspended in 1x PBS (for EdU Alexa Fluor 488 imaging) or BG11M medium (for β-EGFP and SSB-EGFP time-lapse imaging) and 1 μL of resuspended culture was pipetted onto a 6-well glass bottom plate (MatTek Corp., Part Number: P06G-1.5-20-F). The cells were sandwiched between the glass and a small 2% low melting point agarose (LMPA) pad (Thermo Fisher Scientific Inc., Part Number: 16520-050) containing 1x BG11. If multiple strains were imaged in a single experiments, the agar pads were placed near the center of the same well, close to but without touching each other to ensure uniform illumination. The 6-well plate was then placed on an inverted fluorescence microscope (IX-81, Olympus Inc.) equipped with a motorized stage (Prior Scientific Inc.), a 100x oil immersion objective (Olympus Inc.) and an EMCCD camera (Luca, Andor Technology Ltd.). Light sources for growth (660 nm) and fluorescence excitation are provided by LED lights. The ambient light intensities are: LOW = ~16 μE m^{-2} s^{-1}, MED ~ 27 μE m^{-2} s^{-1}, and HIGH ~ 40 μE m^{-2} s^{-1}. Regions of interest (ROIs) encompassing cells from different conditions were recorded, and a 10-mL mixture containing 2% LMPA and 1x BG11 was poured on top of the agarose pad to preventing drying during the

experiment and to provide essential nutrients for time-lapse imaging. EdU-Alexa Fluor 488 imaging began as soon as the LMPA solution solidified. For time-lapse imaging, cells were kept on the microscope for at least 24 hours to allow them to adapt to the microscope environment before imaging began. In glucose-feeding experiments, 4 g/L glucose was added to the solidified LMPA 45–60 minutes before the dark pulse was applied.

Image acquisition was performed using a custom-written script for the μManager software (7). Both EdU Alexa Fluor 488 and EGFP images were captured with a 487 – 513 nm excitation bandpass filter, a 520 nm dichroic filter, and a 528 – 556 nm emission bandpass filter. Exposure times for EdU Alexa Fluor 488 imaging and time-lapse imaging were 1 s and 1.5 s, respectively. To facilitate cell segmentation, one chlorophyll fluorescence image (excitation bandpass filter: 542 – 582 nm, dichroic filter: 593 nm, emission long-pass filter: 593 nm), one in-focus brightfield image and eight slightly defocused brightfield images were also taken for each pre-recorded ROI at each time point. For time-lapse imaging in dark, no bright-field image was taken except at the beginning and at the end of the dark pulse.

Cell segmentation was performed using a custom-written MATLAB program. First, chlorophyll images were used to produce binary masks of cells via Otsu thresholding. Pixels belonging to the foreground are considered as candidate pixels of cells. Next, the in-focus and defocused brightfield images were subject to the transform of intensity equation (TIE) algorithm (8), producing pseudo-phase-contrast images of cells to which the watershed algorithm was then applied to segment cells. Segmented objects lying outside the binary masks were eliminated and erroneous segmentation results were corrected by manually adjusting segmentation parameters. For time-lapse microscopy, stage drift was corrected by calculating the cross-correlation of chlorophyll images between consecutive frames, and cell lineages were constructed by paring detected cells from one frame to another by maximizing the total number of pixels shared between each pair of cells. Cell lengths were typically calculated as the major axis length of the cell shape. In rare cases where cells were either filamentous or highly curved, a backbone-tracing algorithm was used to determine the cell length (9). The presence and positions of EdU and EGFP foci were detected using a digital bandpass filter.

To obtain the apparent dissociation rate of β-EGFP ($\lambda_{\mathrm{app\_diss}}$), nearby β-EGFP foci belonging to the same cell from consecutive frames were linked to create foci trajectories, from which the lifetime of β-EGFP and its survival functions were obtained.

The apparent dissociation of β-EGFP can be modeled as two independent Poisson processes, the photobleaching of EGFP and the physical dissociation of β-EGFP from the replication fork (10). Since all experiments were performed with identical imaging parameters, we interpret different $\lambda_{\mathrm{app\_diss}}$ values measured from different conditions as a result of different physical dissociation rates of β-EGFP.

IV. Determination of replication time by BrdU ChIP-qPCR

To estimate the time it takes to replicate one chromosome, we followed a BrdU ChIP-qPCR protocol modified from previous studies (4, 11) to track the initiation and completion of replication events during the first several hours after cells were transferred from dark to light (Fig. S3). Since BrdU is a thymidine analog like EdU, when cells start replicating, a large amount of BrdU will be incorporated into the genomic DNA (gDNA) near the replication origin (*oriC*) region. When replication events come close to finish, BrdU incorporation will be concentrated near the replication terminus (*ter*) region of the chromosome. The time interval between the *oriC* and *ter* incorporation peaks serves as an estimate of the time it takes to replicate one chromosome. The experimental procedures are detailed below.

Cells incubated in dark for ~18 hours were split into 7 time-point groups and released to constant light condition. For each hour thereafter, cells from one group were pulse-labeled with 300 μM BrdU for 60 minutes before being subject to immunoprecipitation (IP).

To obtain BrdU-labeled regions of the chromosome, gDNA was first extracted using phenol and chloroform and precipitated with ethanol. gDNA was then sheared into ~500 bp fragments using the Covaris S220 sonicator and cleaned up with Qiagen MinElute columns. The size of sheared gDNA fragments was verified with the Agilent 4200 TapeStation. Next, 500 μL IP buffer (10 mM sodium phosphate, pH 7.0, 140 mM sodium chloride, 0.05% Triton X-100) was added to 5 – 7 μg clean gDNA. The solution was boiled at 95 °C for 10 minutes, and chilled on ice for 2

minutes. Biotin-conjugated α-BrdU antibody (Invitrogen) was added at 1:10 (antibody:BrdU) weight ratio and the solution was incubated at room temperature (RT) for 30 minutes with gentle rotation. 30 μL streptavidin-conjugated magnetic beads (Life Technologies) were used to capture the antibody-BrdU complex with a 30-minute incubation at RT. Next, the beads were pelleted with a magnetic stand (Invitrogen), washed with 500 μL IP buffer once, and resuspended with 200 μL digestion buffer (50 mM Tris-HCl, pH 8.0, 10 mM EDTA, 0.5% SDS). The digestion solution was then boiled at 95 °C for 5 minutes to release the antibody-BrdU complex from the beads. After chilling on ice for 2 minutes, 50 μg proteinase K (Ambion) was added to the solution and digestion was carried out overnight at 57 °C with shaking at 1000 rpm. The next day, BrdU-containing fragments were eluted with 2×25 μL water using the Zymo concentrator-5 columns.

To quantify the amount of BrdU-*oriC* and BrdU-*ter* present in the sample, real-time quantitative polymerase chain reaction (qPCR) was performed with primer sets (Table S4) targeting *oriC*-proximal and *ter*-proximal regions of the chromosome. The reactions were performed on a Bio-Rad CFX384 Real-Time PCR Detection System with Roche LightCycler 480 Sybr Green I Master mix, using the following program: 95 °C for 10 minutes, and 45 cycles of [95 °C for 10 seconds, 50 °C for 20 seconds, 72 °C for 20 seconds], followed with melting curve analysis. The absolute copy numbers were obtained from calibration curves generated using standard DNA fragments amplified with primers (Tables S4) that target a ~500 bp region encompassing either *oriC* or *ter* of the chromosome.

The amount of BrdU-*oriC* and BrdU-*ter* amplified from samples pulse-labeled one hour before dark-to-light transfer (t = -1 to 0) were considered background and were subtracted from all subsequent measurements.

The experiment revealed that the copy number of BrdU-*oriC* first became significantly different from the background level (two-tailed t-test, $p < 0.01$) 2 hours after the transfer to constant light, while that of BrdU-*ter* first became significantly different from the background 4 hours post-transfer. We thus estimate that it takes approximately 2 hours to replicate one chromosome under our growth condition.

Deconvolving the EdU vs. θ profile (see the following section) produces a replication initiation curve (Fig. 1E, blue) and a replication completion curve (Fig. 1E, green). The difference between these two curves, which we call the initiation-completion difference curve, depends on the time interval used for deconvolution, which is 2 hours as determined using BrdU ChIP-qPCR. To verify that this 2-hour estimate of replication time is consistent with EdU imaging data, we compared the degree of similarity between the initiation-completion curve and the time-derivative of the EdU vs. θ profile. The idea is that, though obtained through different means, both entities describe the same physical quantity, which is the surplus of replication initiation events (per μm per time interval) to that of replication completion events. Plotting these two curves together (Fig. S4) showed that they are indeed similar in magnitude and shape, supporting the validity of the replication time estimate.

V. Solving replication initiation and completion profiles by deconvolution

The EdU vs. θ plot (Fig. 1C, denoted as g in this section for simplicity) describes the approximate number of active replication events per cell length at a given θ, which is a convolution product between two functions: the rate of replication initiation per cell length (denoted as s in this section), and a boxcar function (denoted as h in this section) with a duration equal to the time it takes to replicate one chromosome:

$$g = s \otimes h \tag{1}$$

g is known and the duration of h is estimated to be 2 hours (see the above section). Therefore, s can be solved using a Wiener filter as (12):

$$S = \left[\frac{1}{H}\frac{|H|^2}{|H|^2 + \eta}\right] G \tag{2}$$

where S, H, and G are Fourier transforms of s, h, and g, respectively. η is the noise-to-signal power ratio, which was estimated as the square of the ratio between the standard deviation and the mean of g.

The replication initiation curve, s, can then be obtained through inverse Fourier transform of S, and the replication completion curve is simply a 2-hour time-delayed version of s.

VI. Stochastic model of DNA replication in dark

Qualitatively, the faster decrease in replication activity in the dark for cells in the subjective daytime state could be a result of faster suppression of new initiation events, more frequent replication failure events, or a combination of both. The goal of performing mathematical modeling is to test which scenario is quantitatively consistent with experimental data. To this end, we modeled replication in the dark with three pathways: replication initiation, fork progression and replicative abortion, where the rates of initiation decay and replicative abortion were both allowed to depend on the clock state at lights-off (θ_{dark}). We then simulated replication events based on the model and different parameter sets and compared the simulation results with experiment ones. The best-fit parameter set should inform us about the clock-dependency of these pathways.

Conceptually, the simulation was done one cell at a time using a proposed parameter set. When a cell is transferred from constant light to dark at a given θ_{dark}, it can have 0 or 1 pre-existing, partially replicated chromosome that needed to be finished in the dark. In addition, depending on λ_{ini}, which describes how fast the initiation rate k_{ini} drops in the dark, the cell may stochastically initiate new rounds of replication. Also, each replication event can potentially abort stochastically, depending on the abortion rate k_{abort}. Replication events in 50 cells of a given θ_{dark} were simulated, and the total number of replication events was normalized by the total length of these cells, producing a simulated version of the "focus density" (counts/μm) as a function of time in the dark. After cells from all 12 clock phases (θ_{dark} = 0, 2, …, 22 hours) were simulated, the overall agreement between the 12 simulated foci time traces and the experimental ones was quantified, followed with another iteration of simulation with a different parameter set. The goal was to perform these steps iteratively with different parameter sets to identify a parameter set that maximizes the overall agreement between the simulated and the experimental focus density data. 50 Markov chains with different starting parameters each undergoing 20000 iterations of parameter optimization were run, and the parameter set that best recapitulated the experimental data was recorded for each chain. Below we describe the technical details of the simulation procedure.

(i) Instantiation of cell population: 12 cell populations of 12 different θ_{dark} values (0, 2, … 22 hours), each composed of 50 cells of an average length of 3 μm, were instantiated at $t = 0$, the onset of dark. The average number of replication events per cell length was set to the experimentally observed β-EGFP density at $t = 0$ (alternatively, the replication event density at $t = 0$ could be set to the EdU density at LL and the simulation results were both qualitatively and quantitatively similar). For a given replication event that is ongoing at lights-out at θ_{dark}, the probability of this replication event being initiated at an earlier subjective time θ_{ini} was drawn according to the following probability distribution function:

$$p(\theta_{\mathrm{ini}}) = \frac{k_{ini}(\theta)}{\int_{\theta_{\mathrm{dark}}-\tau}^{\theta_{\mathrm{dark}}} k_{ini}(\theta)d\theta} \tag{3}$$

Where τ is the two-hour replication time window (using other values of $\tau \leq 4$ hours did not significantly change model predictions), and $k_{ini}(\theta)$ is the initiation rate for a given θ, estimated by deconvolving the β-EGFP focus density vs. θ profile at $t = 0$ using the two-hour replication time window. The number of remaining base pairs still needed to be replicated in the dark is thus equal to:

$$bp = \Omega \times \frac{\tau - \delta\theta}{\tau} \tag{4}$$

where $\delta\theta$ is the time lag between θ_{ini} and θ_{dark}, and $\Omega = 2.7 \times 10^6\ bp$ is the *S. elongatus* genome size.

(ii) Initiation: initiation event was modeled as an inhomogeneous Poisson process, where the rate of initiation decays exponentially in the dark:

$$k_{ini} = k_{ini,t=0}\, e^{-\lambda_{ini}\, t} \tag{5}$$

The ansatz $e^{-\lambda_{ini}\, t}$ was chosen to reflect the intuition that available resources decay as the night progresses. λ_{ini} is the decay rate of the initiation rate in the dark. λ_{ini} was allowed to be clock-dependent, i.e., each focus density time trace has its own λ_{ini}. Consecutive initiation events were simulated numerically using the thinning method (13), until the sum of all interarrival times exceeded the duration of the dark pulse.

(iii) Fork progression: the time required to finish replicating a chromosome equals to the number of base pairs to be replicated divided by the fork speed (bp/s). Based on the 2-hour estimate of replication time, the fork speed should be around 375 bp/s in LL. To account for potential slowing down or reversible fork stalling due to resource limitation in the dark, we used a search window between 50 bp/s and 400 bp/s for the fork speed in the model.

(iv) Abortion: abortion events were modeled as a homogenous Poisson process, with a rate constant k_{abort} that was either dependent on θ_{dark} (full model) or independent of it (reduced model). The distribution of arrival times for abortion events has an exact solution:

$$\tau_{abort} = \frac{-1}{k_{abort}} \ln(U) \tag{6}$$

where U is the uniform distribution between 0 and 1. The arrival time of each abortion event was drawn from this distribution directly.

Based on the framework above, each cell needs to complete a total of $N \geq 0$ replication events in the dark, where N includes pre-existing, partially completed event as well as newly initiated replication rounds. Replication events are independent from each other. For each replication event, the time it takes to complete (τ_{rep}) is calculated from (iii), and the time it takes to abort (τ_{abort}) is obtained from (iv). Active replication takes place during the time window between t_{ini} and $t_{ini} + \min[\tau_{rep},\ \tau_{abort}]$, where t_{ini} is the time of initiation for the replication event being considered.

In each iteration of the Markov chain, new parameters were drawn from Gaussian-shaped proposal distributions centered at the current parameter set. Replication events were simulated using the new parameters, and the total number of ongoing replication events at each time point were divided by the sum of cell lengths, producing a simulated replication density time trace over the course of the dark pulse, denoted as $Y_{\mathrm{sim}}(t, \theta_{\mathrm{dark}})$, where $\theta_{\mathrm{dark}} = 0, 2, \ldots, 22$ hours. Each of the 12 $Y_{\mathrm{sim}}(t, \theta_{\mathrm{dark}})$ time traces was compared to the corresponding β-EGFP density

time trace collected experimentally, denoted as $Y_{\exp}(t, \theta_{\text{dark}})$, and the overall goodness-of-fit of iteration i was quantified as the average Poisson-weighted residual sum of squares:

$$r_i = \frac{1}{12^2} \sum_{\theta} \sqrt{\sum_{t} \frac{1}{Y_{\exp}(t, \theta_{\text{dark}})} \left[Y_{\text{sim}}(t, \theta_{\text{dark}}) - Y_{\exp}(t, \theta_{\text{dark}}) \right]^2} \quad (7)$$

where a lower value of r_i indicates a better fit. The parameter set of the i^{th} iteration was accepted with a probability of $\left(\frac{r_{i-1}}{r_i}\right)^{\beta}$, where the hyperparameter β was set to a relatively high value of 50 to help prevent the chain from wandering too far from the current best parameter set. Accepted parameter values were designated as the current parameter set, which served as the mean values of proposal distributions for the next iteration. The sampling parameters and the best parameter values for the full model (mean of 50 Markov chains) are given in Table S5.

The model-predicted $ter/oriC$ ratio in the dark was calculated as $\frac{N_{nr}+N_{ter}}{N_{nr}+N_{partial}+N_{oriC}}$, where N_{nr} is the number of non-replicating chromosomes at the onset of dark that each contributes an equal number of $oriC$ and ter, assumed to be 3–6 per cell for cells of an average length of 3 μm (14). $N_{partial}$ is the number of partially replicated chromosomes at the onset of dark that each contributes 1 $oriC$ but no ter. N_{oriC} and N_{ter} are newly replicated $oriC$ and ter in the dark up to time t.

VII. Determination of *ter/oriC* ratio by qPCR

To investigate whether cells were able to complete replications in dark, we performed qPCR to track the ratio between *ter*-proximal and *oriC*-proximal regions (*ter/oriC* ratio) as a function of time in the dark for cells given either an in-phase dark pulse (θ_{dark} = 12 hr) or an out-of-phase one (θ_{dark} = 0 hr). Cell cultures entrained at the two clock phases were each split into 7 time-point groups. Cells were harvested and their gDNA purified after *t* = 0, 2, 4, 6, 8, 10, 12 hours of incubation in the dark. gDNA was sheared into ~500 bp fragments using the Covaris S220 sonicator and the sheared fragment size was cleaned up using Qiagen MinElute columns. The *ter/oriC* ratio for each condition at each time point was determined by performing qPCR over the

sheared gDNA. The primers and thermocycler settings used for amplifying the *ter*-proximal and *oriC*-proximal regions were identical to those for the BrdU ChIP-qPCR experiments (see section IV and Table S4).

VIII. dNTP measurements

Two batches of cell cultures were entrained such that at the time of harvest, they are at subjective dawn and subjective dusk respectively. The cultures were adjusted to the same OD_{750} of 0.7 before harvest. 35 mL culture from each batch were harvested and concentrated at 4 °C with centrifuge. Extraction was performed by adding 400 μL of cold 80% methanol to the pellet which were then stored at -80 °C. After 1 hour, 600 μL chloroform was added and the mixture was vortexed at 3000 rpm for 7 minutes and chilled on ice for 2 minutes. Next, 500 μL water was added to the mixture which were then vortexed for another 7 minutes at 3000 rpm. Finally, the organic layer and the aqueous layer were separated by centrifuging at 20000 rpm at 4 °C for 15 minutes. The top 800 μL aqueous layer were collected. To speed up evaporation and minimize the number of freeze-thaw cycles later, the collected aqueous layer was partitioned into 100 μL aliquots, concentrated overnight with SpeedVac at 45 °C, and reconstituted with 25 μL water. Reconstituted samples were flash frozen in liquid nitrogen and stored at -80°C until future use.

dNTP quantification was performed using a fluorescence primer extension assay (15) that is an improved version of the original probe-hydrolysis-based assay (16). By supplying a single-stranded DNA template, a template-annealing primer, dNTP mix (excluding the dNTP to be measured), DNA-intercalating dye EvaGreen and Q5 polymerase, the template can be converted to double-stranded DNA products that will render EvaGreen fluorescent. The number of converted products and thus the fluorescence signal are proportional to the amount of the limiting dNTP present in the reconstituted cell extracts. Measured fluorescence is converted to picomoles of the limiting dNTP using pre-established calibration curves generated from standard solutions of known concentrations of each limiting dNTP.

The assay was set up following the original paper by Purhonen et al. (15), with the only modification that a hot-start version of the Q5 polymerase was used with 30 seconds of polymerase activation at 95 °C at the beginning of the assay. Purhonen et al. offered two

different approaches for quantifying the fluorescence signal from converted products, using either the background-subtracted end-point fluorescence readout, or the fluorescence change at the melting point of the converted product (Δfluorescence/Δ°C). We took the latter approach as it offered better signal-to-noise ratios.

We measured on the microscope that the cell density is approximately 10^{10} cells per liter at OD_{750} = 0.7. Assuming the volume of each cell is 1.92 fL (3 μm × 0.8 μm × 0.8 μm), the measured picomoles of dNTP were converted to concentration. Spiking cell concentrates with known quantities of dNTPs and performing the same extraction and dNTP quantification procedures, we estimated that the dNTP recovery rate was ~55%, and the reported dNTP concentrations were scaled up accordingly.

IX. Supplementary Data Figures

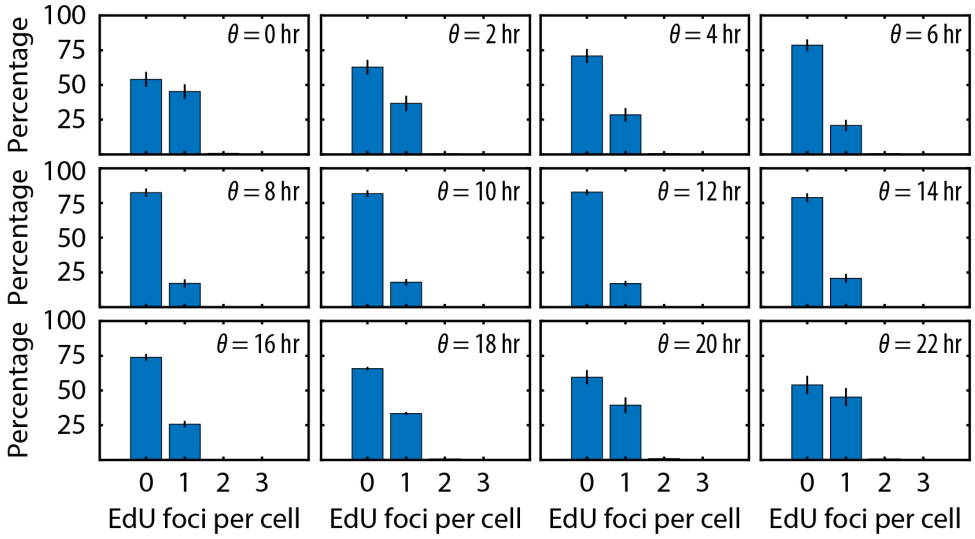

Fig. S1. The number of EdU fluorescent spot per cell. Approximately 700 cells were analyzed for each θ. Error bars are SEMs from three independent experiments.

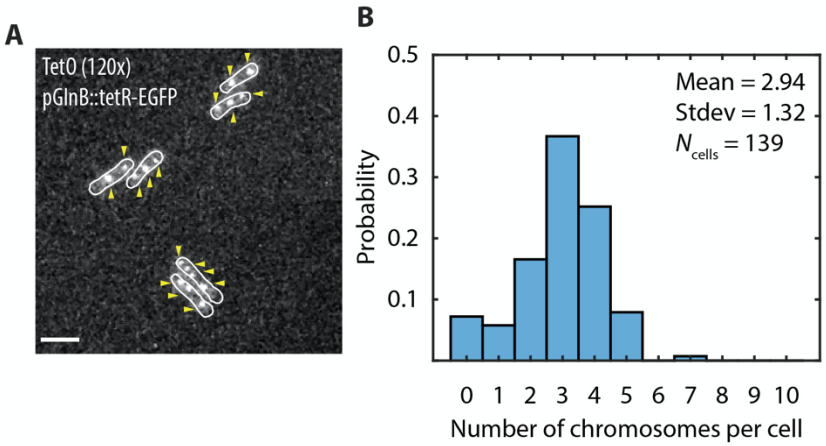

Fig. S2 (A) Cyanobacteria typically contain multiple copies of chromosomes per cell. (*A*) Visualization of individual genomic loci in single cells using the Tet repressor-operator system. Tandem arrays of *tet* operator sites (120x TetO) are integrated into the chromosome ~213° from the replication origin. Constitutively expressed and EGFP-tagged repressor protein TetR binds to the operator arrays, which allows for visualization of individual chromosomes (14, 17). Scale bar = 3 μm. (*B*) Histogram of chromosome counts per cell quantified from TetO/TetR-EGFP images. 7% of cells did not contain any signal due to the presence of unlabeled cells (see SI Appendix, section I).

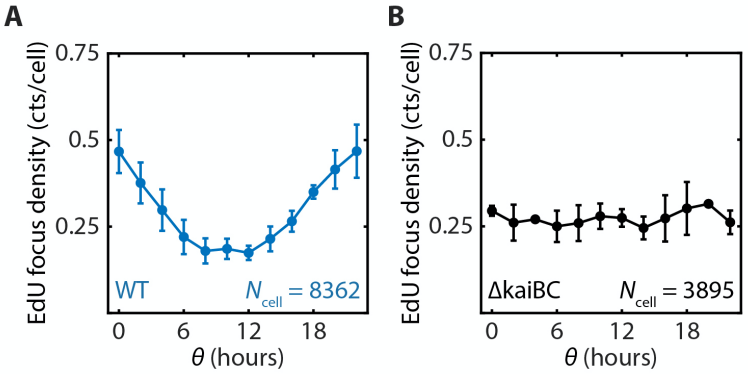

Fig. S3. EdU densities normalized by cell counts**.** (*A*) EdU focus densities (counts per cell) as a function of θ in WT cells. (*B*) EdU focus densities (counts per cell) as a function of θ in Δ*kaiBC* cells. Error bars are SEMs from three independent experiments.

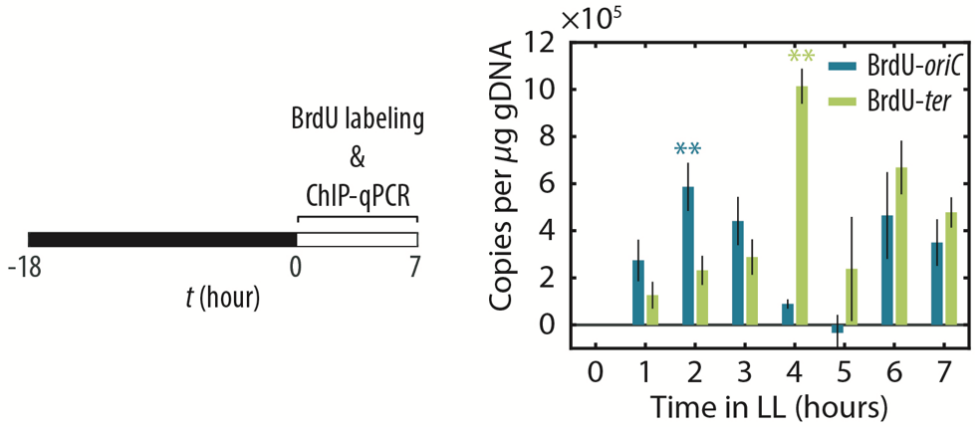

Fig. S4. Estimation of the time required to replicate one chromosome. ChIP-qPCR was performed to quantify the amount of newly incorporated BrdU-*oriC* and BrdU-*ter* as a function of time since cells were transferred from dark to constant light condition. The copy number of each amplicon present right before the transfer (at 0 hr) is considered as background and subtracted for all subsequent time points. Error bars are SEMs from three independent experiments. **denotes the first time point where the amount of BrdU-*oriC* or BrdU-*ter* is significantly ($p < 0.01$) different from the background.

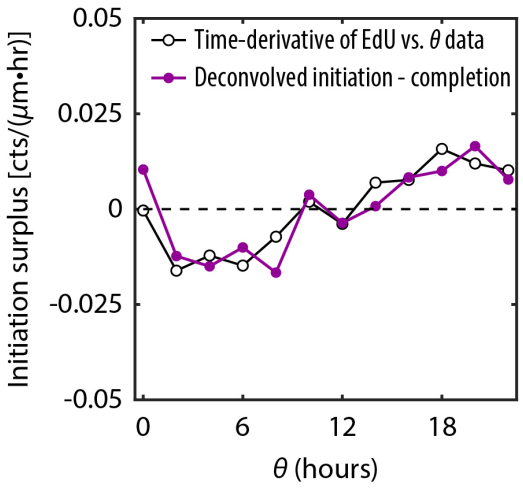

Fig. S5. Validation of the replication time estimate. (Purple curve) the difference between the deconvolved replication initiation profile and completion profile (i.e., the difference between the blue and the green curves in Fig. 1E), plotted against the time-derivative of the EdU density vs. θ profile (black curve). The overall shape and magnitude of the initiation-completion difference curve agrees with those of the derivative curve, supporting the validity of the replication time estimate (Fig. S4).

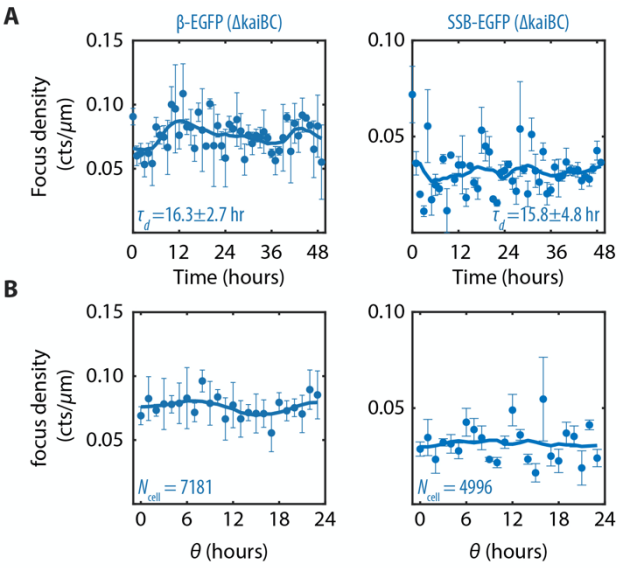

Fig. S6. (*A*) Average β-EGFP and SSB-EGFP focus densities in Δ*kaiBC* background as a function of time in LL, under intermediate (MED) illumination level. Solid lines are seven-point running average and error bars are SEMs from three independent experiments. (*B*) Focus densities as a function of θ. No circadian rhythm is observed for either replisome component.

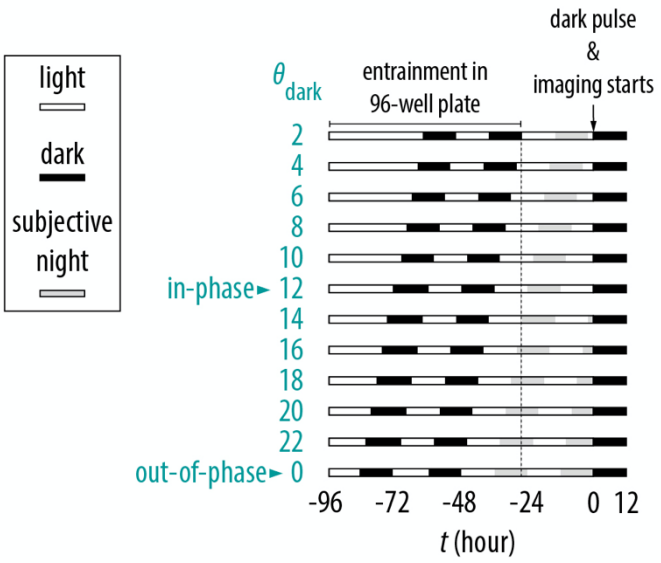

Fig. S7. Schematic diagram showing the entrainment procedure for replisome imaging in dark. 12 samples were entrained with programmable LED arrays attached to a 96-well plate, such that clock phases were 2 hours apart from each other. By the time the entrainment for the last group ($\theta_{\mathrm{dark}} = 2$) was finished (indicated by the vertical dashed line), all samples were loaded to the microscope where cells had 24 hours to adapt to the microscope environment before a 12-hour dark pulse was applied at $t = 0$. Fluorescence images were recorded for each sample at every hour during the dark pulse, for a total of 12 hours.

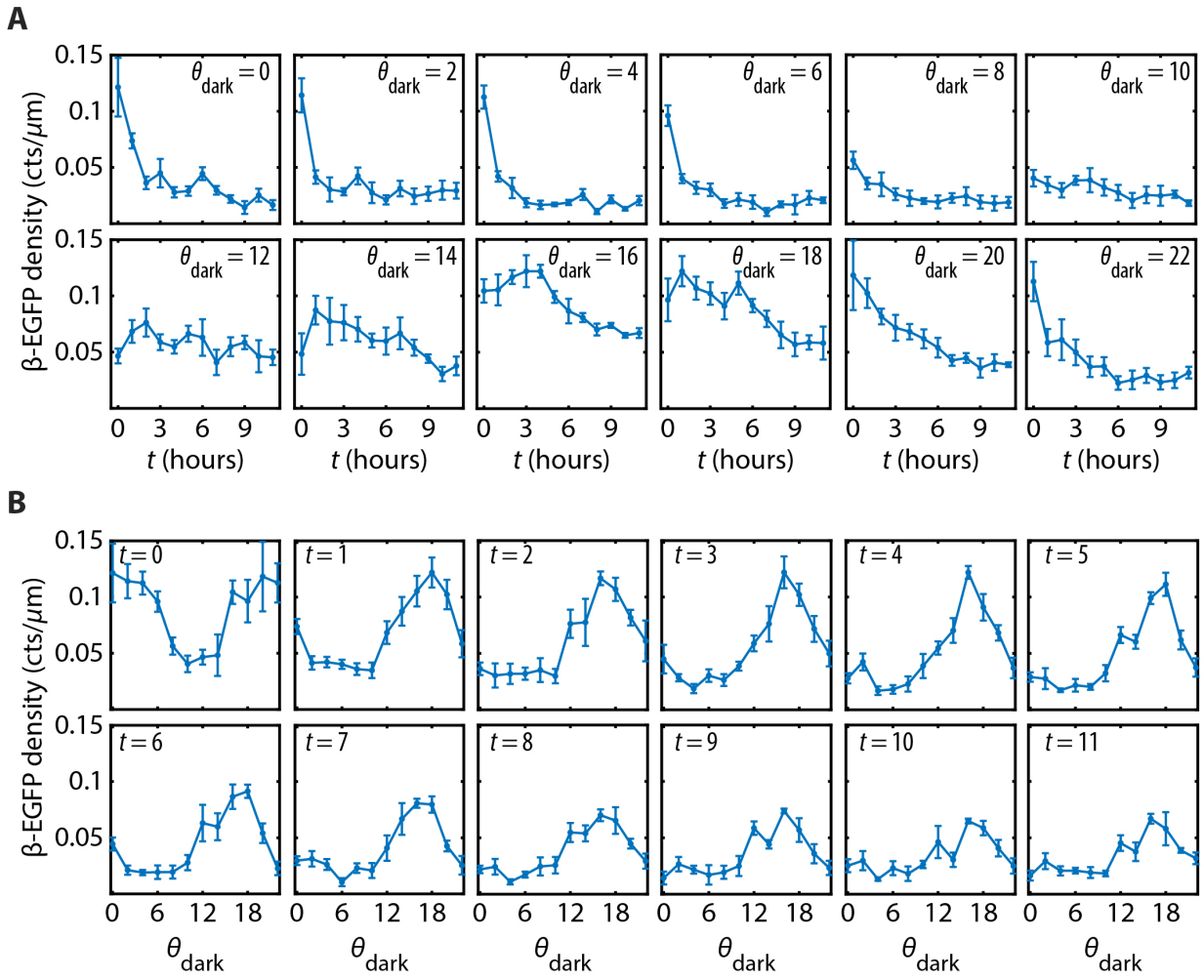

Fig. S8. β-EGFP focus densities (WT background) in the dark. (*A*) β-EGFP focus densities plotted as a function of time in the dark (t), for cells of different clock states (θ_{dark}). (*B*) The same data plotted as a function θ_{dark}, at different time points in the dark. Error bars are SEMs from five independent experiments totaling ~27000 cells.

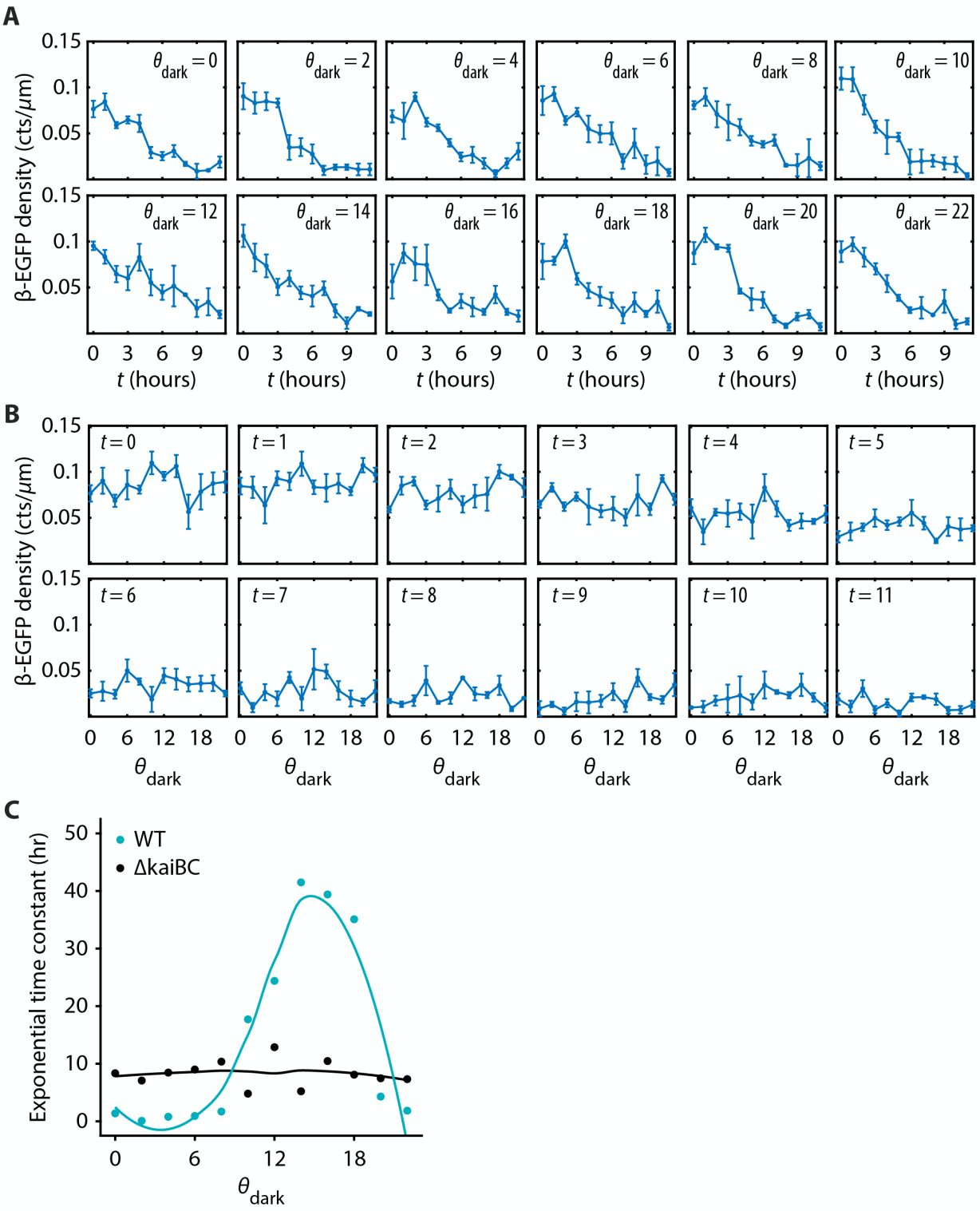

Fig. S9. β-EGFP focus densities (Δ*kaiBC* background) in the dark. (*A*) β-EGFP focus densities plotted as a function of time in the dark (t), for cells of different θ_{dark}. (*B*) The same data plotted as a function θ_{dark}, at different time points in the dark. Error bars are SEMs from four

independent experiments totaling 11380 cells. (*C*) Exponential time constants obtained by fitting β-EGFP focus densities vs. time in dark to a single-term exponential decay function. Solid lines are trendlines by local regression. As expected for Δ*kaiBC* cells, β-EGFP densities decay in the dark in a θ_{dark}-independent manner.

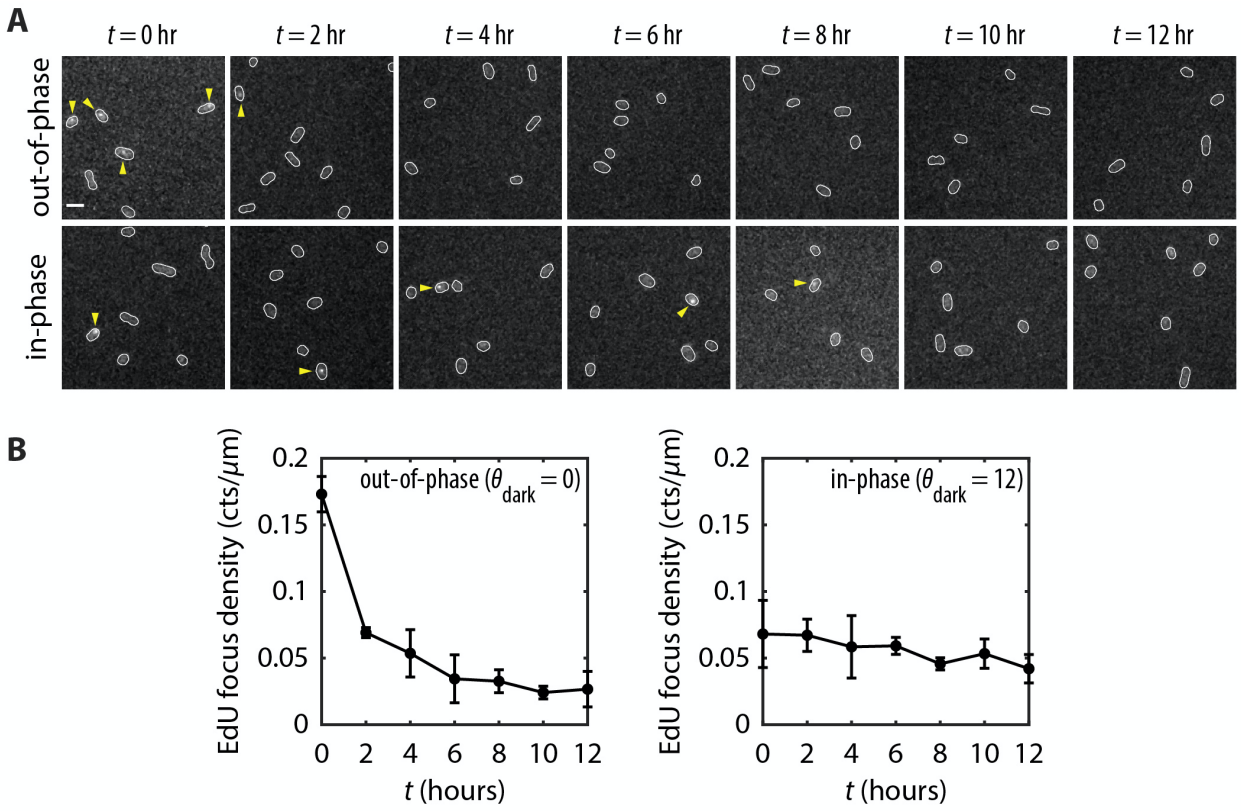

Fig. S10. DNA replication in the dark for cells with clock states out-of-phase and in-phase with the onset of the dark pulse. (*A*) Fluorescence images showing EdU Alexa Fluor 488 foci in cells from the out-of-phase group ($\theta_{\mathrm{dark}} = 0$) or the in-phase-group ($\theta_{\mathrm{dark}} = 12$) with a 12-hour dark pulse. Scale bar = 3 μm. (*B*) EdU densities as a function of time in the dark. The values correspond to the number of active replication events per μm of cell length during a 10-minute pulse-labeling time window centered at each t. Error bars are SEMs from three independent experiments totaling ~3000 cells.

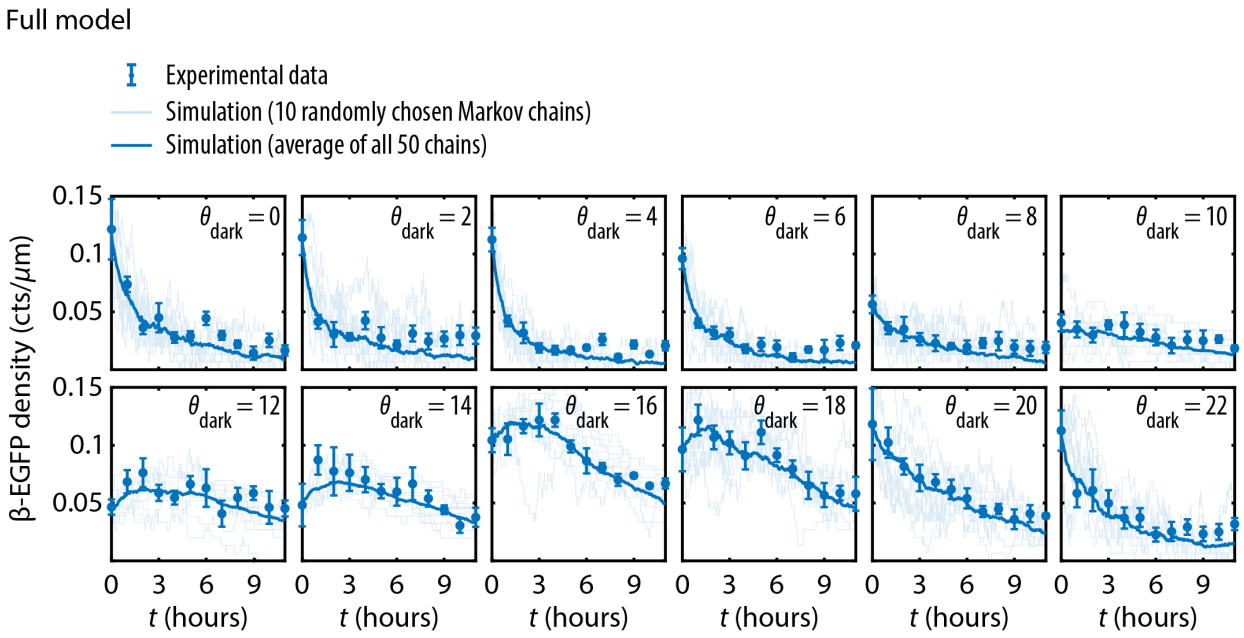

Fig. S11. Fitting experimental data to the replication model. Simulated replication events (counts/μm) plotted against experimentally collected β-EGFP data in dark, for various θ_{dark} values. Simulation was based on the full model, where both λ_{ini} and k_{abort} were allowed to have clock-dependency. The best-fit λ_{ini} values are largely clock-invariant, but the best-fit k_{abort} values exhibit circadian dependence and peak near subjective dawn (Fig. 3F), suggesting that a roughly uniform initiation decay rate across θ_{dark} and higher abortion rates near subjective dawn could potentially explain the observed clock-dependent decay of replication events in the dark.

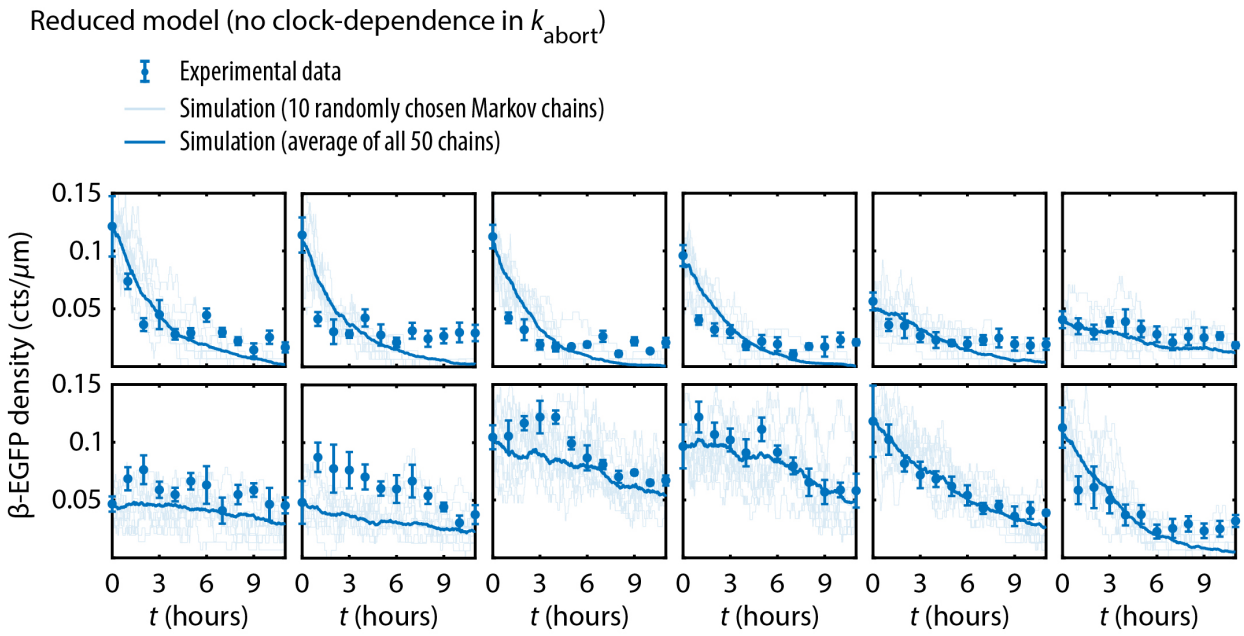

Fig. S12. Fitting replication data to a replication model with a clock-independent abortion rate. Simulated replication events (counts/μm) plotted against experimentally collected β-EGFP data in dark, for various θ_{dark} values. Simulation is based on the reduced model, where λ_{ini} is clock-dependent but cells of all θ_{dark} have the same abortion rate. The best fits have large discrepancies with experimental data. *F*-test suggested that the full model is strongly preferred over the reduced model (*p*-value ≈ 0).

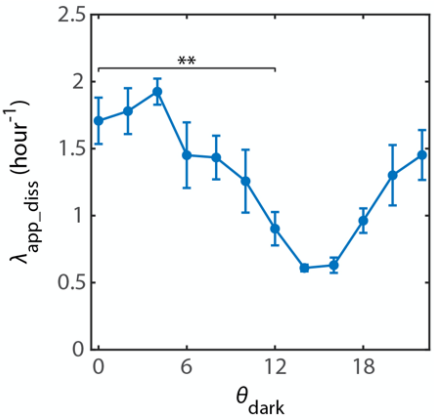

Fig. S13. Apparent dissociation rate constants $(\lambda_{\mathrm{app\_diss}})$ of β-EGFP in the dark for cells of different (θ_{dark}). Error bars are SEMs from five independent experiments. $^{**}p < 0.01$ between the in-phase $(\theta_{\mathrm{dark}} = 12)$ and the out-of-phase $(\theta_{\mathrm{dark}} = 0)$ groups (two-sample *t*-test).

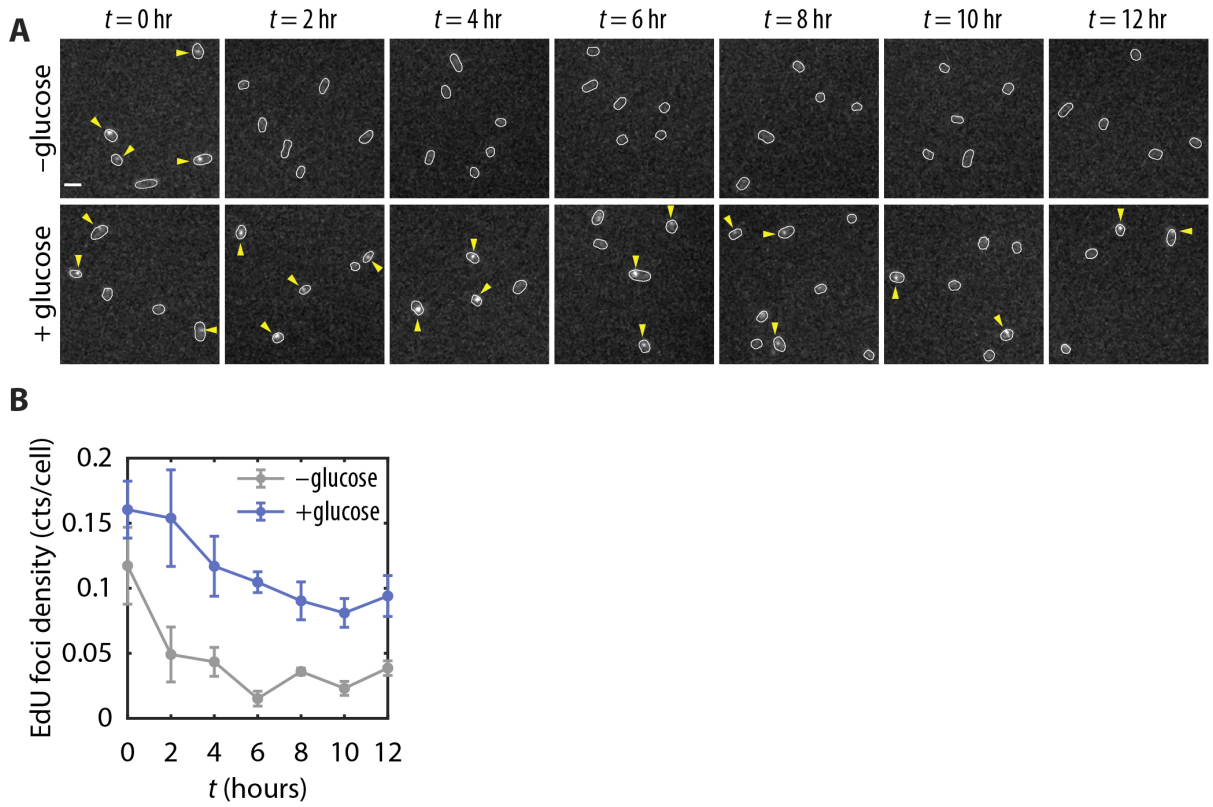

Fig. S14. DNA replication in GalP-expressing cells in the dark. (*A*) Fluorescence images showing EdU Alexa Fluor 488 foci in GalP-expressing cells subject to a 12-hour, out-of-phase dark pulse, without (–) or with (+) glucose supplemented before the dark. Scale bar = 3 μm. (*B*) EdU densities as a function of time in the dark for untreated and glucose-treated cells. Error bars are SEMs from two (–glucose) or three (+glucose) independent experiments totaling ~3000 cells.

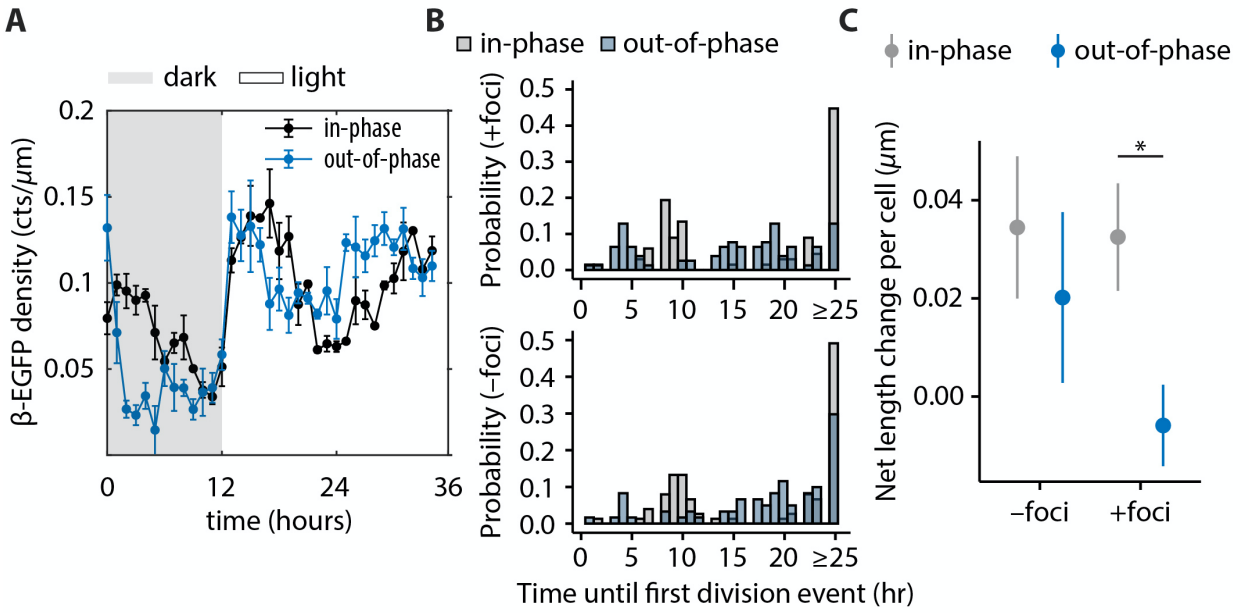

Fig. S15. Characterization of replication, division and growth for in-phase and out-of-phase cells during and after a 12-hour dark pulse. (*A*) β-EGFP density time traces during and after the dark pulse. Error bars are SEMs from three independent experiments. (*B*) Histograms showing the amount of time it took for in-phase and out-of-phase cells to divide again after being released to constant light, plotted separately for cells that were actively replicating ("+foci") when the lights were turned off (top panel), and for those that were not replicating at lights-off ("-foci", bottom panel). $N_{\text{in-phase}}$ = 172 cells and $N_{\text{out-of-phase}}$ = 167 cells. (*C*) The net change in cell length per cell from the onset of dark to one hour post-dark. Negative values correspond to cells experiencing an overall shrinking of cell size during this time period. Out-of-phase cells that were actively replicating at lights-off ("+foci", blue) on average gained less biomass compared to in-phase cells ("+foci", grey) (two-tailed *p*-value = 0.04907, vs. *p*-value = 0.3174 for "-foci" group). Error bars are SEMs from three biological replicates.

X. SI Tables

Table S1. Strains used in this study

Strain	Description	Plasmids used*	Resistance	Source
MRC1122	pTrc::Thymidine Kinase-HA in WT background		Sp, Strp	(4)
MRC1211	SSB-EGFP in WT background	pMR0208	Sp, Strp	This work
MRC1212	β-EGFP in WT background	pMR0209	Sp, Strp	This work
MRC1213	β-EGFP in Δ*kaiBC* background	pMR0209, MR0091	Sp, Strp, Gm	This work
MRC1214	β-EGFP in Δ*sasA* background	pMR0209, MR0092	Sp, Strp, Gm	This work
MRC1215	pTrc::Thymidine Kinase-HA in Δ*kaiBC* background	pMR0091 transformed into MRC1122	Sp, Strp, Gm	This work
MRC1216	pGlnB::GalP in thymidine kinase background	pMR0210 transformed into MRC1122	Kan, Sp, Strp	This work
MRC1217	pGlnB::GalP in β-EGFP background	pMR0210 transformed into MRC1212	Kan, Sp, Strp	This work
MRC1218	SSB-EGFP in Δ*kaiBC* background	pMR0208, MR0091	Sp, Strp, Gm	This work
MRC1219	pGln::tetR-EGFP	pMR0211	Sp, Strp	This work
MRC1220	TetO/pGln::tetR-EGFP	pMR0212 transformed into MRC1219	Kan, Sp, Strp	This work

*Plasmids used to create the corresponding strain from WT unless noted otherwise

Abbreviations of antibiotics
Sp: spectinomycin
Strp: streptomycin
Gm: gentamicin
Kan: kanamycin

Table S2. Plasmid used in this study

Plasmid	Description	Resistance	Source
pBSK(+)	pBlueScript II SK (+), vector backbone for making fluorescent reporter constructs	carbenicillin	Agilent
pLAU44	Source of tetO arrays	Gm	(18)
EB2072	Source of tetR	Sp, Strp	(17)
pAM1303	Neutral-site I (NS1) integration plasmid	Sp, Strp	(19)
pAM1579	Neutral-site II (NS2.1) integration plasmid	Kan	(20)
pAM2314	Source of spectinomycin resistance cassette	Sp, Strp	(21)
pMR0091	*kaiBC* knockout plasmid	Gm	(22)
pMR0092	*sasA* knockout plasmid	Gm	(22)
pMR0208	SSB-EGFP-Sp^R (with upstream and downstream flanking regions) inserted into pBSK(+)	Sp, Strp	This work
pMR0209	β-EGFP-Sp^R (with upstream and downstream flanking regions) inserted into pBSK(+)	Sp, Strp	This work
pMR0210	pGlnB::GalP inserted between SalI and XbaI restriction sites of pAM1579	Kan	This work
pMR0211	pGln::tetR-EGFP inserted between NotI and SacI restriction sites of pAM1303	Sp, Strp	This work
pMR0212	120xTetO + Kan^R (with upstream and downstream flanking regions), inserted between SacI and NotI restriction sites of pBSK(+)	Kan	This work

Table S3. Primers used for strain construction

Plasmid	Forward and reverse primer sequences (5' to 3')	Amplified Product
pMR0208	(F)CCCCCGGGCTGCAGGAATTCTGCGTTTGACGGCTTCCACA (R)CCGCCGCCGAACAGATCGCTGTCTGGATCG	1 kb upstream of *ssb* + *ssb*
	(F)TCTGTTCGGCGGCGGCG (R)GCAGGCATGTTACTTGTACAGCTCGTCCATG	Gly-Gly-Gly-Gly-Ser linker + *egfp*
	(F)TACAAGTAACATGCCTGCAGGTCGACT (R)GTCGAGGGATTATTTGCCGACTACCTTGGTGAT	Spectinomycin resistance cassette
	(F)GGCAAATAATCCCTCGACTCCAAGGCTCAA (R)GTATCGATAAGCTTGATATCGAATTCGCTGGCGGGGATGCT	1 kb downstream of *ssb*
pMR0209	(F)CCCCCGGGCTGCAGGAATTCATTCTTTGACCAAGGATCAGGACTTAAC (R)CCGCCGCCGCTGCGCAACTGAATCGG	1 kb upstream of *dnaN* + *dnaN*
	(F)ATTCAGTTGCGCAGCGGCGGCGGCG (R)GATCTCAACTTTATTTGCCGACTACCTTGGTGATCT	Gly-Gly-Gly-Gly-Ser linker + *egfp* + Sp^R (amplified from pMR0208)
	(F)CGGCAAATAAAGTTGAGATCCCCTTTTTCTCACC (R)GTATCGATAAGCTTGATATCGAATTCTTTGATGCCCTCACCAGC	1 kb downstream of *dnaN*
pMR0210	(F)ACGGGTAACCGATATCGTCGACCTTAAGGTCAATCGCTTTTGGATTGACTATG (R)CGTCAGGCATTTTTTTTCCTCCTTAGGGAACTCTCC	pGlnB promoter with C-terminal ribosome-binding site
	(F)GGAAAAAAAATGCCTGACGCTAAAAAACAGG (R)TAGCTCGAGCCCGGGTCTAGATTAATCGTGAGCGCCTATTTCGC	GalP

Plasmid	Forward and reverse primer sequences (5' to 3')	Amplified Product
pMR0211	(F)CATACTAGAGGATCGGCGGCCGCTTAAGGTCAATCGCTTTTGGATTGAC (R)TAATCTAGACATTTTTTTTCCTCCTTAGGGAACTCTCCTTAAGCCAGGG	pGlnB promoter with C-terminal ribosome-binding site
	(F)GGAGGAAAAAAAAATGTCTAGATTAGATAAAAGTAAAGTGATTAACAG (R)GCTCACCATAGACCCACTTTCAC	tetR
	(F)GTGGGTCTATGGTGAGCAAGGGCGAG (R)GCTCGAAATTCGAGCTCTTACTTGTACAGCTCGTCCATGCC	*egfp*
pMR0212	(F)GAACAAAAGCTGGAGCTCGCAACTATCCCTCGATCAACGT (R)GTGCTAGATGGGAGGCATTAGAAGCATCATC	1.5 kb upstream flanking sequence
	(F)GCCTCCCATCTAGCACTGGCGGGGGTCC (R)CCAGGCATTCCCAGTCACGACGTTGTAAAACGAC	120x TetO array
	(F)ACTGGGAATGCCTGGCAGTTCCCTAC (R)TTCAATCCGCATTAGAAAAACTCATCGAGCATCAAATGAAAC	Kan^R cassette
	(F)GTTTTTCTAATGCGGATTGAAATTGTTCAACACG (R)GATCCACTAGTTCTAGAGCGGCCGCGTTCTCGACCACCCATTCAGCA	1.5 kb downstream flanking sequence

Table S4. qPCR primers

Target region	Forward and reverse primer sequences (5' to 3')	Notes
oriC	(F)CAGTGCTACGATGCTTTGG (R)GACAGACTGGTATTCAGTTCG	
Ter	(F)TCGAAATAAGAACCGAACTGG (R)ATTACTTCTTAATCGCTCTCACC	
oriC	(F)TTCAGTCTGTGGAGAAAGGAAC (R)AGGCGCGAAACGATATCG	For calibration
Ter	(F)AGCCACTTTCAAACCTTTCTAG (R)ACTGGGGTTATGAGTTACTAGATG	For calibration

Table S5. Sampling parameters and best-fit values for the replication model

Parameter		Sampling parameters			Best-fit values*
Name	Unit	Lower bound	Upper bound	Proposal distribution width	
fork speed	bp/s	50	400	20	83±15
k_{abort}†	hr^{-1}	0	3	0.1	1.743±0.177
					2.160±0.147
					2.087±0.151
					2.078±0.143
					1.569±0.204
					0.711±0.170
					0.223±0.072
					0.189±0.062
					0.278±0.060
					0.553±0.090
					0.953±0.126
					1.574±0.173
λ_{ini}†	hr^{-1}	0	1	0.1	0.266±0.056
					0.250±0.055
					0.345±0.065
					0.344±0.063
					0.271±0.059
					0.299±0.072
					0.396±0.077
					0.358±0.071
					0.393±0.080
					0.273±0.075
					0.193±0.050
					0.281±0.073

*Mean ± 95% CI.

†Best-fit values are listed in ascending order of θ_{dark} (0, 2, …, 22 hours).

References

1. S. S. Golden, J. Brusslan, R. Haselkorn, Expression of a family of psbA genes encoding a photosystem II polypeptide in the cyanobacterium Anacystis nidulans R2. *EMBO J* **5**, 2789-2798 (1986).
2. D. G. Gibson *et al.*, Enzymatic assembly of DNA molecules up to several hundred kilobases. *Nature methods* **6**, 343-345 (2009).
3. R. Reyes-Lamothe, D. J. Sherratt, M. C. Leake, Stoichiometry and architecture of active DNA replication machinery in Escherichia coli. *Science* **328**, 498-501 (2010).
4. S. Watanabe *et al.*, Light-dependent and asynchronous replication of cyanobacterial multi-copy chromosomes. *Molecular microbiology* **83**, 856-865 (2012).
5. E. Leypunskiy *et al.*, The cyanobacterial circadian clock follows midday in vivo and in vitro. *Elife* **6**, e23539 (2017).
6. A. Salic, T. J. Mitchison, A chemical method for fast and sensitive detection of DNA synthesis in vivo. *Proceedings of the National Academy of Sciences of the United States of America* **105**, 2415-2420 (2008).
7. A. D. Edelstein *et al.*, Advanced methods of microscope control using muManager software. *J Biol Methods* **1**, 10 (2014).
8. L. Waller, L. Tian, G. Barbastathis, Transport of Intensity phase-amplitude imaging with higher order intensity derivatives. *Opt Express* **18**, 12552-12561 (2010).
9. Y. Liao, M. J. Rust, The Min Oscillator Defines Sites of Asymmetric Cell Division in Cyanobacteria during Stress Recovery. *Cell Syst* **7**, 471-481 (2018).
10. J. C. Gebhardt *et al.*, Single-molecule imaging of transcription factor binding to DNA in live mammalian cells. *Nature methods* **10**, 421-426 (2013).
11. C. Marchal *et al.*, Genome-wide analysis of replication timing by next-generation sequencing with E/L Repli-seq. *Nat Protoc* **13**, 819-839 (2018).
12. N. Wiener, *Extrapolation, interpolation, and smoothing of stationary time series, with engineering applications* (Technology Press of the Massachusetts Institute of Technology, Cambridge, 1949), pp. ix, 163 p.
13. P. A. W. Lewis, G. S. Shedler, Simulation of Nonhomogeneous Poisson Processes by Thinning. *Nav Res Log* **26**, 403-413 (1979).
14. A. H. Chen, B. Afonso, P. A. Silver, D. F. Savage, Spatial and temporal organization of chromosome duplication and segregation in the cyanobacterium Synechococcus elongatus PCC 7942. *PLoS One* **7**, e47837 (2012).
15. J. Purhonen, R. Banerjee, A. E. McDonald, V. Fellman, J. Kallijarvi, A sensitive assay for dNTPs based on long synthetic oligonucleotides, EvaGreen dye and inhibitor-resistant high-fidelity DNA polymerase. *Nucleic acids research* (2020).
16. P. M. Wilson *et al.*, A novel fluorescence-based assay for the rapid detection and quantification of cellular deoxyribonucleoside triphosphates. *Nucleic acids research* **39**, e112 (2011).
17. I. H. Jain, V. Vijayan, E. K. O'Shea, Spatial ordering of chromosomes enhances the fidelity of chromosome partitioning in cyanobacteria. *Proc Natl Acad Sci U S A* **109**, 13638-13643 (2012).
18. I. F. Lau *et al.*, Spatial and temporal organization of replicating Escherichia coli chromosomes. *Mol Microbiol* **49**, 731-743 (2003).

19. R. D. Kulkarni, S. S. Golden, mRNA stability is regulated by a coding-region element and the unique 5' untranslated leader sequences of the three Synechococcus psbA transcripts. *Molecular microbiology* **24**, 1131-1142 (1997).
20. C. R. Andersson *et al.*, Application of bioluminescence to the study of circadian rhythms in cyanobacteria. *Methods Enzymol* **305**, 527-542 (2000).
21. J. L. Ditty, S. R. Canales, B. E. Anderson, S. B. Williams, S. S. Golden, Stability of the Synechococcus elongatus PCC 7942 circadian clock under directed anti-phase expression of the kai genes. *Microbiology* **151**, 2605-2613 (2005).
22. G. K. Pattanayak, C. Phong, M. J. Rust, Rhythms in Energy Storage Control the Ability of the Cyanobacterial Circadian Clock to Reset. *Current Biology* **24**, 1934-1938 (2014).